



**HAL**  
open science

## Stacking faults density driven collapse of magnetic energy in hcp -cobalt nano-magnets

H T T Nong, K Mrad, F Schoenstein, J-Y Piquemal, N Jouini, B Leridon, S Mercone

► **To cite this version:**

H T T Nong, K Mrad, F Schoenstein, J-Y Piquemal, N Jouini, et al.. Stacking faults density driven collapse of magnetic energy in hcp -cobalt nano-magnets. *Advances in Natural Sciences: Nanoscience and Nanotechnology*, 2017, 8 (2), pp.025012. 10.1088/2043-6254/aa5e1e . hal-04188842

**HAL Id: hal-04188842**

**<https://hal.science/hal-04188842v1>**

Submitted on 27 Aug 2023

**HAL** is a multi-disciplinary open access archive for the deposit and dissemination of scientific research documents, whether they are published or not. The documents may come from teaching and research institutions in France or abroad, or from public or private research centers.

L'archive ouverte pluridisciplinaire **HAL**, est destinée au dépôt et à la diffusion de documents scientifiques de niveau recherche, publiés ou non, émanant des établissements d'enseignement et de recherche français ou étrangers, des laboratoires publics ou privés.

# Stacking faults density driven collapse of magnetic energy in *hcp*-cobalt nano-magnets\*

H T T Nong<sup>1</sup>, K Mrad<sup>1</sup>, F Schoenstein<sup>1</sup>, J-Y Piquemal<sup>2</sup>, N Jouini<sup>1</sup>, B Leridon<sup>3</sup> and S Mercone<sup>1</sup>

<sup>1</sup> Laboratoire des Sciences des Procédés et des Matériaux, Université Paris Nord, Sorbonne Paris Cité, CNRS UPR-3407, 99, Av. J. B. Clément, 93430 Villetaneuse, France

<sup>2</sup> Interfaces Traitements Organisation et Dynamique des Systèmes, Université Paris Diderot, Sorbonne Paris Cité, CNRS UMR 7086, 15 rue J. A. de Baïf, 75205 Paris Cedex 13, France

<sup>3</sup> LPEM-ESPCI Paris, PSL Research University, CNRS, Sorbonne Université, UMPC, 10 Rue Vauquelin, F-75005 Paris, France

E-mail: [thi.nong@lspm.cnrs.fr](mailto:thi.nong@lspm.cnrs.fr)

Received 12 December 2016

Accepted for publication 9 January 2017

Published 9 May 2017



## Abstract

Cobalt nanowires with different shape parameters were synthesized via the polyol process. By calculating the magnetic energy product ( $BH_{\max}$ ) both for dried nano-powder and for nanowires in their synthesis solution, we observed unexpected independent  $BH_{\max}$  values from the nanowires shape. A good alignment of the nanowires leads to a higher  $BH_{\max}$  value. Our results show that the key parameter driving the magnetic energy product of the cobalt nanowires is the stacking fault density. An exponential collapse of the magnetic energy is observed at very low percentage of structural faults. Cobalt nanowires with almost perfect *hcp* crystalline structures should present high magnetic energy, which is promising for application in rare earth-free permanent magnets.


Keywords: nanowire, magnetic energy, stacking faults, *hcp* cobalt

Classification numbers: 4.08, 5.02

## 1. Introduction

A good understanding of the correlation between the structural and magnetic properties of Co-based nanostructures is mandatory for the improvement of their applications in magnetic recording media [1–3], as well as in permanent magnet systems [4–6]. In both kinds of applications high magnetocrystalline anisotropy is crucial in order to maintain stability in the written information and high energy product. Thus, a cobalt pure hexagonal close-packed (*hcp*-cobalt) structure is strongly required for maximizing this magnetocrystalline anisotropy as it shows (compared to the cobalt cubic one) the highest anisotropy constant (i.e. in bulk  $k_1 = 450 \text{ kJ m}^{-3}$ ). Unfortunately, the *hcp*-cobalt structure is also known to easily present regular occurrence of growth faulting [7, 8]. A

stacking fault in the *hcp* structure creates layers of atoms presenting a face-centered cubic (*fcc*) symmetry which is magnetically more isotropic (i.e. in bulk  $k_1 = 63 \text{ kJ m}^{-3}$ ). Three different kinds of stacking faults are commonly observed to occur: *intrinsic*, *extrinsic* and *twin-like* types [9]. They have a detrimental overall effect on the magnetic properties of Co-based hexagonal systems, usually resulting in a macroscopic lower anisotropy and thus in a magnetic softening [10, 11]. Theoretical studies [9] demonstrated that the magnetocrystalline anisotropy energy (MAE) in a *hcp*-Co structure strongly depends on the probability and type of growth faulting. The dependence appears not to be simply the sum of the changes in the magnetocrystalline anisotropy energy due to each individual stacking fault. In fact, the long-ranged oscillations predicted in the MAE by the presence of each stacking fault indicate that the situation is far more complex.

 Original content from this work may be used under the terms of the [Creative Commons Attribution 3.0 licence](https://creativecommons.org/licenses/by/3.0/). Any further distribution of this work must maintain attribution to the author(s) and the title of the work, journal citation and DOI.

\* Oral talk at 8th International Workshop on Advanced Materials Science and Nanotechnology (IWAMSN2016), 8–12 November 2016, Ha Long City, Vietnam.

This long-ranged behavior could give rise to significant finite-size effects in nano-sized samples and have strong consequences on their magnetic properties. Experimentally, the presence of stacking faults is normally quantified in terms of the stacking fault density, which is partly a measure of how close the stacking faults are located. This long-range behavior suggests that in small systems, even for low density of stacking faults, the effect of the local breaking of the uniaxial symmetry should reduce the magnetic anisotropy, causing thermal instability and low switching field.

Sokalski *et al* [12] experimentally found on Co-based thin films a strong linear decrease of the uniaxial anisotropy constant versus the increasing *c*-axis value. Such a trend was already reported previously in the literature [13, 14] and qualitatively consistent with bulk measurements of magnetostriction for cobalt single crystal, where a compression of the *c*-axis increases the magnetic anisotropy. However, they found a clear non-linear dependence of the magnetic anisotropy constant on the stacking fault density indicating that these could have an indirect effect on magnetic anisotropy via their influence on the crystallographic lattice parameter. Mai *et al* [15] found in CoNi nanowires a linear dependence of the coercive field on the stacking faults density. In this work the shape contribution to the switching field has been kept constant, thus suggesting a linear correlation of the magneto-crystalline contribution with the density of stacking faults. It is also worth mentioning that in some hexagonal Cobalt nanoalloys (e.g. SmCo<sub>5,7</sub>) [16, 17] small amounts of defects seem to improve the magnetic properties. All these results suggest that the influence of the stacking fault effects on the properties of metal nanostructures is quite controversial.

Keeping in mind the potential application of cobalt nanowires as building blocks in permanent magnets that is clearly connected with the mandatory optimization of their magnetic energy product and anisotropy, we address here the complete study of the stacking fault effects over the magnetic energy of *hcp*-cobalt nanowires. Our results indicate that the stacking faults induced by the elaboration conditions strongly determine the structural and magnetic properties of *hcp*-Co. Comparing our results to the recent ones of Gandha *et al* [18] on the effect of shape dispersion on the maximization of the magnetic energy product, we could hence conclude that appropriate control of the stacking faults can lead to the improvement of the magnetic properties much stronger than the shape anisotropy.

## 2. Experimental

Cobalt nanowires were prepared by the reduction of metallic salts in a liquid polyol [19, 20]. This method allows accurate control of the nanoparticles' size and morphology via kinetic control of the growth step [21]. The nanowires' powder was separated from the solution by centrifugation washed several times by ethanol and then dried in a vacuum oven at 50 °C. Standard TEM imaging has been performed by using JEOL-2011 operating at 200kV for all the elaborated systems in order to study the morphology and size dispersion of the

nano-objects. Four morphological parameters have been taken into account: the diameter (*D*), the length (*L*), the width of the head (*W*), and the thickness (*T*) of the head (see figure 1(b)). Accurate measurements of these four morphological parameters have been performed by measuring more than 150 pictured nanowires per batch. The crystallographic structure and density of stacking faults have been characterized by x-ray diffraction (XRD) patterns (not shown here) recorded with a PANalytical Empyrean diffractometer equipped with Cu-K $\alpha$  x-ray source ( $\lambda = 1.5406 \text{ \AA}$ ). Elaboration details as well as TEM and XRD analyses will be published elsewhere [22]. The magnetic energy product of the Co nanowires has been calculated from the static magnetic measurements using a Quantum Design MPMS 3 magnetometer. For this purpose we recorded magnetic hysteresis cycles by field cooling (FC) the samples under the application of  $H = 70 \text{ kOe}$  at different temperatures. For each batch (i.e. each morphology), we measured the magnetic properties of the nanowires inside their synthesis solution (polyol) and their corresponding dried powder. In the case of nanowires inside the polyol solution, the FC procedure allows a huge percentage of nanowires aligning along the applied magnetic field before the polyol solution freezes (i.e.  $T_G = 220 \text{ K}$ ). In the case of the powder, we blocked the dried nanowires inside an epoxy resin whose solidification is operational at room temperature.

## 3. Results and discussion

Figure 1(a) presents the typical nanowires morphology observed in our systems by TEM. All the samples studied here are constituted of nanowires having a mean diameter (*D*) in the range of 17–26 nm and a mean length (*L*) of 89 nm up to 276 nm (see figure 1(b)). They present an elongated morphology with a mean thickness (*T*) of the head ranging between 11.2 to 52.3 nm and with a mean width (*W*) of 24 to 33 nm (see figure 1(b)). Morphology details can be also found in table 1.

We show typical observed normalized FC hysteresis loops in figures 1(c) and (d) respectively for the nanowires in their polyol solution and their corresponding dried powder. The squareness of the hysteresis loop of the polyol samples is better than the one of the corresponding powder. Considering the  $M_r/M_s$  ratio (i.e. the magnetic remanence at  $H = 0 \text{ Oe}$  over the saturation magnetization), we found this ratio equal to 0.9 for the nanowires inside their polyol solution and equal to 0.5 for the corresponding blocked powder. This confirms the good alignment of the nanowires when they freeze in their synthesis solution under the application of a magnetic field [23]. In fact, in this latter condition, dipolar interactions between the nanowires are negligible and they are better dispersed. Thus the nanowires can easily align along the external magnetic field applied during the freezing leading to a higher squareness of the magnetic loop (i.e. higher  $M_r/M_s$  ratio) [26]. The  $M_r/M_s$  ratio of 0.5 observed in the case of the powder confirms the random orientation of the nanowires blocked in the epoxy resin used to immobilize the particles during the measurements. Comparing all the measured hysteresis

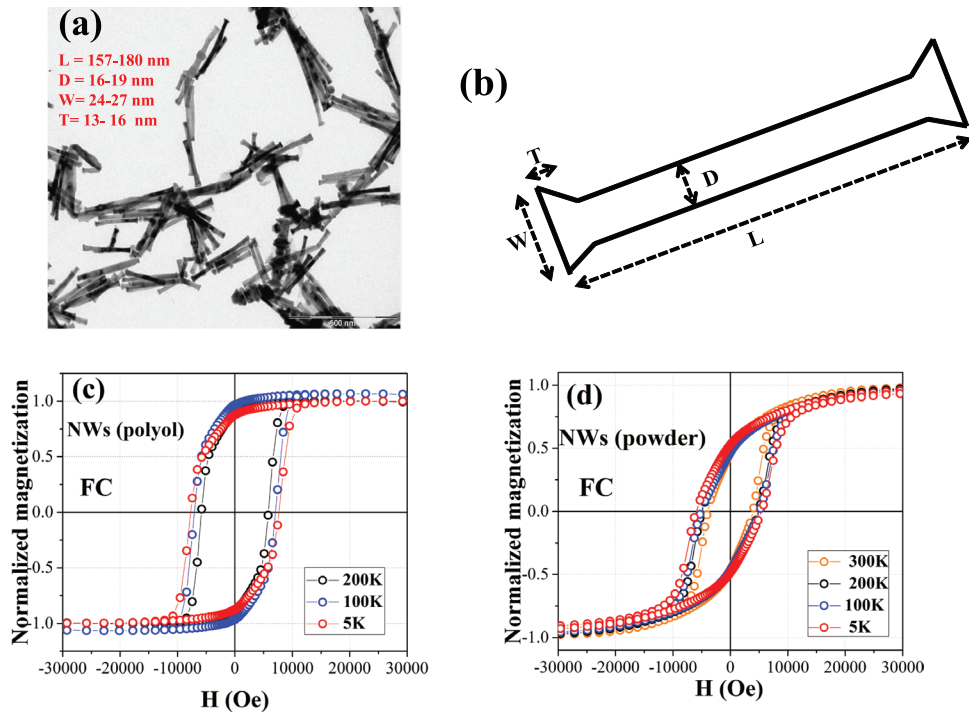


**Figure 1.** TEM image of Co nanowires having morphological parameters:  $L = 157\text{--}180\text{ nm}$ ,  $D = 16\text{--}19\text{ nm}$ ,  $W = 24\text{--}27\text{ nm}$  and  $T = 13\text{--}16\text{ nm}$  (a); sketch of morphological relevant parameters for Co nanowires (b); hysteresis cycles at different temperatures of the nanowires imaged inside their polyol solution (c) and as dried powder (d).

**Table 1.** Morphology details ( $L/D$ ,  $D/W$  and  $T$ ) of several studied batches, magnetic parameters at low temperature (5 K) for both nanowires in their polyol solution and as dried powder.

$L/D$	$D/W$	$T$ (nm)	$SQ$ powder	$\alpha$ powder	$M_r/M_s$		$H_c$ (Oe)		$M_s$ (emu g $^{-1}$ )	$\delta$
					Polyol	Powder	Polyol	Powder		
4.29	0.77	12.86	0.42	2.39	0.65	0.621	7659	5231	157	—
6.38	0.69	11.84	0.21	2.21	0.53	0.455	6779	4954	136	0.082
7.34	0.75	14.17	0.27	1.05	0.64	0.48	6382	5790	133	0.063
9.16	0.88	11.20	0.23	2.73	—	0.44	6456	4120	149	0.074
10.26	0.65	19.73	0.31	2.43	0.87	0.53	7674	5640	169	0.050
10.70	0.78	52.36	0.28	1.27	—	0.48	7130	5240	143	0.056
12.23	0.74	18.86	0.27	1.90	0.76	0.48	7275	5769	141	0.054

cycles, we could not verify the expected influence of the size and the shape of Co nanowires on their magnetic properties. As reported previously [23–25], the coercive behavior of the nanowires is expected to increase with the increase of the  $L/D$  ratio and it is supposed to show a non-linear behavior as a function of the thickness  $T$ . This suggested that, in our case, other parameters should be responsible for the observed magnetic properties. Good candidates have been proposed in the literature [12, 15] as the dispersion of the size and the stacking fault density. Thus, in order to detect the relevant parameter driving the magnetic behavior of these nanowires, we decided to calculate from the measured hysteresis loops the magnetic energy product for each batch ( $BH_{\max}$ ). We used the following equations reported in literature [18]:

$$BH_{\max} = \begin{cases} B_r^2/[4\mu_0(1+\alpha)] & \text{if } \mu_0 H_c \geq B_r/[2(1+\alpha)] \\ H_c[B_r - \mu_0(1+\alpha)H_c] & \text{if } \mu_0 H_c \leq B_r/[2(1+\alpha)] \end{cases}, \quad (1)$$

where  $B_r = 4\pi M_r D$  (Gauss) is the magnetic flux density through the structure at the remanent state,  $D = 8.92\text{ g cm}^{-3}$  the cobalt bulk density,  $\mu_0$  is the magnetic permeability of the vacuum,  $H_c$  (Oe) the measured coercive field and  $\alpha = 2M_r(1 - SQ)/H_c$  (dimensionless). This latter coefficient shows how the magnetic energy product  $BH_{\max}$  strongly depends on the squareness ( $SQ$ ) of the nanowires hysteresis loop. The  $SQ$  is defined as  $SQ = \frac{A}{H_c M_s}$ , where  $A$  is the area under the second quadrant of the loop (see figure 2),  $H_c$  (Oe) and  $M_s$  (emu g $^{-1}$ ) are respectively the coercive field and the magnetization at saturation. The final  $BH_{\max}$  product has been converted from MGOe in the CGS system to kJ m $^{-3}$  in the international system of units.

Obviously, the calculation of the magnetization at saturation was possible only in the case of the powder samples which we could weigh before blocking into the epoxy. In the case of the nanowires in polyol we could not do this. To give a first estimation of the magnetic energy product also in this latter case, we decided to calculate the  $BH_{\max}$  by using simple

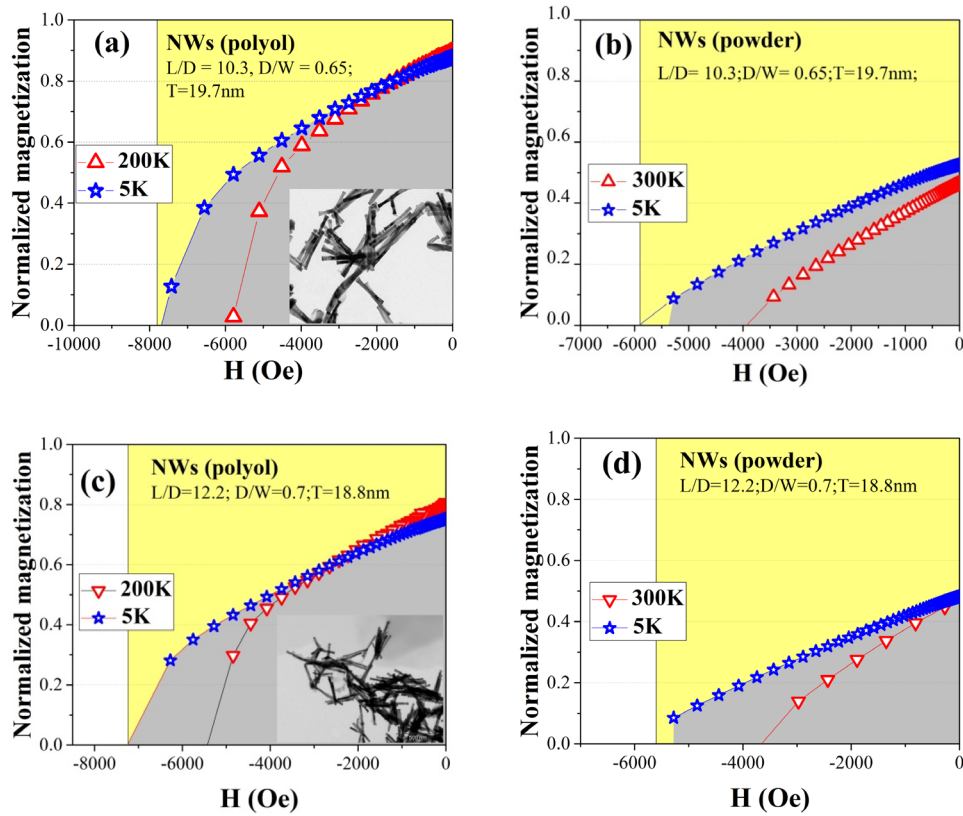


**Figure 2.** The second quadrant of hysteresis loop for (a) Co nanowire in polyol with  $D$  (16–19 nm),  $L$  (157–180 nm),  $W$  (24–27 nm),  $T$  (13–16 nm) and the corresponding powder (b); second quadrant of hysteresis loop for (c) Co nanowire in polyol with  $D$  (18–21 nm),  $L$  (214–259 nm),  $W$  (22–25 nm),  $T$  (15–18 nm) and the corresponding powder (d).

considerations on the measured hysteresis loops. For all our samples the condition  $\mu_0 H_c \geq B_r/[2(1 + \alpha)]$  is verified. It can be deduced from equation (1) that the ratio between the magnetic energy product of the same batch of nanowires inside their synthesis solution to the one of their corresponding dried powder (i.e.  $BH_{\max}(\text{polyol})/BH_{\max}(\text{powder})$ ) is proportional to the ratio between the corresponding areas under the hysteresis loop in the second quadrant (grey area in figure 2). So after normalizing the hysteresis curves in order to make them comparable, we easily deduced the ratio of those areas:

$$\frac{S_{\text{polyol}}}{S_{\text{powder}}} = a \approx \frac{BH_{\max}(\text{polyol})}{BH_{\max}(\text{powder})}, \quad (2)$$

where  $S_{\text{polyol}}$ ,  $S_{\text{powder}}$  are the area under the second quadrant of the hysteresis curve respectively of nanowires in polyol and their corresponding powder samples. Figures 2(a) and (c) show a normalized second quadrant for two different batches of nanowires inside their synthesis solution both at high and low temperatures. A normalized second quadrant of the corresponding powders is shown in figures 2(b) and (d). From figure 2, it is easy to deduce that the area under the curve decreases considerably when the nanowires are dried (in powders). This behavior can be attributed to the random alignment and high dipolar interactions of the latter compared to their corresponding nanowires inside the polyol solution. As the  $M_r/M_s$  ratio and the  $H_c$  strongly affect the  $BH_{\max}$  value, we expect the alignment and dispersion of the nanowires to be key parameters to improve the magnetic energy product. In fact, as

presented before, the  $BH_{\max}$  in equations (1) and (2) strongly depends on the squareness of the hysteresis loop and thus from the area under the second quadrant of this cycle. We found that for a quite equal diameter in the middle of the nanowire ( $D = 16\text{--}21$  nm), the squareness value of the second quadrant is not higher in the case of the longer nanowire ( $L = 214\text{--}259$  nm) compared to ( $L = 157\text{--}180$  nm) (see figures 2(a) and (c)), suggesting again that a more relevant parameter is playing an important role on the magnetic energy product instead of the morphology.

It has already been reported [23] that the shape's parameters drive not only the coercive field but also the easiness of the alignment of the nanowires. Thus our results seem to go against these previous observations. In order to go deeper into this odd shape effect observed over the magnetic energy product, we studied the  $BH_{\max}$  behavior as a function of the relevant morphological parameter (i.e.  $L/D$ ,  $D/W$  and  $T$ ) (shown in figure 3). It is important to underline that we show here only the morphology results for nano-powder samples, as we found exactly the same trend for the corresponding nanowires inside the synthesis solution. Thus, these latter results would be redundant.

As expected, better performances of the magnetic energy product are obtained at low temperature (figure 3) for each morphology. This cannot be attributed to the shape contribution to the reversal mechanism of the nanowires (i.e.  $H_{\text{shape}}$ ) as this doesn't change in function of temperature. Considering a simple model in which the shape anisotropy contribution to the coercive

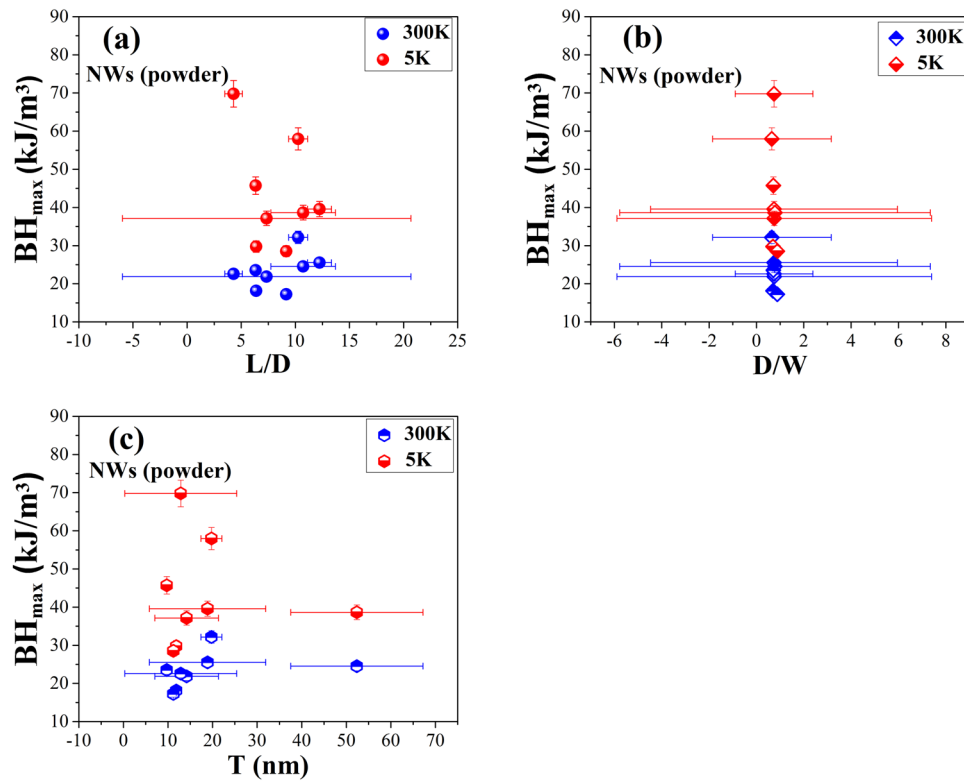


**Figure 3.**  $BH_{max}$  as a function of (a)  $L/D$ , (b)  $D/W$  and (c)  $T$ . The non-homogeneity of the nanowires was a reason for reducing the  $BH_{max}$ .

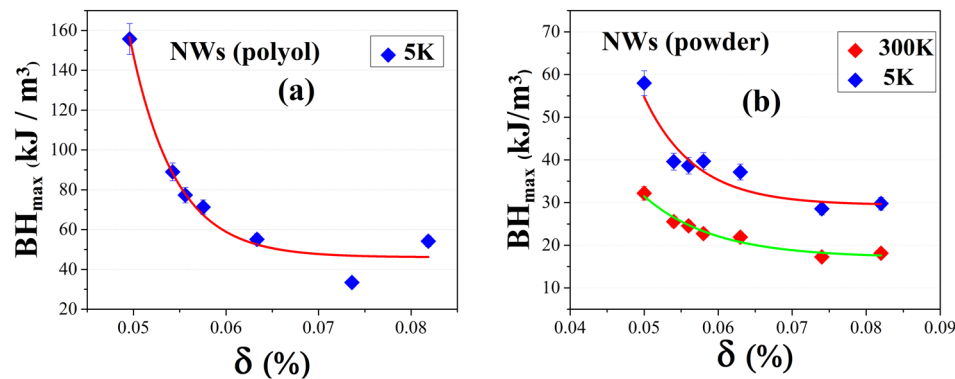


**Figure 4.**  $BH_{max}$  of Co nanowires as a function of stacking fault density, (a) polyol sample, (b) powder sample. The lines (green and red for 300K and 5K, respectively) are exponential fits showing the rapid decrease of  $BH_{max}$  with the increasing of stacking fault density.

field of the nanowires is added to the magnetocrystalline contribution (i.e.  $H_c \sim H_{\text{shape}} + H_{\text{MC}}$ , being  $H_{\text{MC}} = 2K_1/M_s$ ) [16, 23], then a higher value of the magnetocrystalline anisotropy constant ( $k_1$ ) expected at low temperature will lead to a higher value of the coercive field [16]. As a result, a higher magnetic energy product is observed at low temperature. The striking feature of the graphs in figure 3 is the absence of any clear dependence of the magnetic energy product to the morphology variations, strongly suggesting that a more relevant parameter is driving the magnetic energy of the *hcp* Co nanowires. Also, comparing our results with the literature we cannot again see any coherence between the magnetic energy product value and the polydispersity of nanowires size [18]. In our case, the polydispersed nanowires (see big error bars in figure 3) do not present the lowest magnetic energy value. It is worth noting that our higher magnetic energy product at room temperature is significantly lower ( $35 \text{ kJ m}^{-3}$ ) than the highest values achieved in

[18] (i.e.  $350 \text{ kJ m}^{-3}$  for monodispersed cobalt nano-powders and  $278.5 \text{ kJ m}^{-3}$  for the poly-dispersed one). To go further, we reported in figure 4 the  $BH_{max}$  dependence on the stacking fault density  $\delta$  for both nanowires inside their polyol solutions (figure 4(a)) and the corresponding powder (figure 4(b)). This density has been calculated for each batch by XRD analysis [19] (details are reported elsewhere [22]). As stated previously [9–14], the stacking fault density,  $\delta$ , strongly affects the magnetocrystalline anisotropy of Co *hcp* nanowires. Sokalski *et al* [12], reported on an important decrease (exponential-like decay) of the magnetocrystalline anisotropy constant with the increasing of stacking fault density in cobalt thin films. Looking into our results in figures 4(a) and (b), we found the exponential decay being coherent also in the case of nano-objects (green and red lines).

The striking feature in figure 4 is that, no matter what the dispersion and morphology of the nanowires, the

stacking fault density drives exponentially the collapse of the magnetic energy product. The exponential decay factor  $c$  ( $BH_{\max} = Ae^{-xc}$  where  $x$  is the stacking fault density) is expected to be affected by the dipolar interactions between nanowires. We could observe a more rapid decay (i.e. higher  $c$ ) in the case of more interacting nanowires.

#### 4. Conclusion

We succeeded in investigating the effect of stacking faults over the magnetic energy product behavior in *hcp*-cobalt nanowires. We compared Co nanowires showing hexagonal crystal symmetry, various sizes and shapes, and different density values of grown faults. The experimental study of the static magnetic properties confirmed that the reversal mechanism in these nanowires depends on both morphological characteristics and structural defects. The magnetic energy product ( $BH_{\max}$ ) behavior as a function of the relevant morphological parameter (i.e.  $L/D$ ,  $D/W$  and  $T$ ) shows better performances at low temperature for each morphology. A higher magnetic energy product is observed at low temperature due to the magnetocrystalline anisotropy contribution to the reversal mechanisms of the nanowires magnetization. The striking feature is the absence of any clear dependence of the magnetic energy product to the morphology variations, strongly suggesting that a more relevant parameter is driving the magnetic energy of the *hcp* Co nanowires. We found that no matter what the dispersion and morphology of the nanowires, the stacking faults play a key role on the observed collapse of the magnetic energy product values. The higher the stacking faults defects, the lower the magnetic energy product.

#### Acknowledgments

H T T Nong thanks USPC IDEX Project ArchiMEdes for the PhD grant support. The magnetic measurements at ESPCI have been supported through Grants from Region Ile-de-France. Agence Nationale de la Recherche and Commissariat à l'Investissement d'Avenir are gratefully acknowledged for their financial support of this work through Labex SEAM (Science and Engineering for Advanced Materials and Devices), ANR 11 LABX 086, ANR 11 IDEX 05 02.5.

#### References

[1] Piramanayagam S N and Srinivasan K 2009 *J. Magn. Mater.* **321** 485

- [2] Choe G, Zheng M, Achaya B R, Abarra E N and Zhou J N 2005 *IEEE Trans. Magn.* **41** 3172
- [3] Lu B, Klemmer T, Wierman K, Ju G, Weller D, Roy A G, Laughlin D E, Chang C and Ranjan R 2002 *J. Appl. Phys.* **9** 10
- [4] Gutfleisch O, Willard M A, Brück E, Chen C H, Sankar S G and Liu J P 2011 *Adv. Mater.* **23** 821
- [5] Poudyal N and Liu J P 2013 *J. Phys. D: Appl. Phys.* **46** 043001
- [6] Fang W, Panagiotopoulos I, Ott F, Boue F, Ait-Atmane K, Piquemal J Y, Viau G and Dalmas F 2014 *J. Nanopart.* **16** 2265
- [7] Mitra G B and Halder N C 1964 *Acta Cryst.* **17** 817
- [8] Sort J, Surinach S, Muñoz J S, Wojcik M, Jedryka E, Nadolski S, Sheludko N and Nogues J 2003 *Phys. Rev. B* **68** 014421
- [9] Aas C J, Szunyogh L, Evans R F L and Chantrell R W 2013 *J. Phys.: Condens. Matter* **25** 296006
- [10] Meier J, Doudin B and Ansermet J P 1996 *J. Appl. Phys.* **79** 6010
- [11] Sun L, Hao Y, Chien C L and Searson P C 2005 *IBM J. Res. Dev.* **49** 1
- [12] Sokalski V, Laughlin D E and Zhu J G 2011 *J. Appl. Phys.* **110** 093919
- [13] Shimatsu T, Sato H, Okazaki Y, Aoi H, Muraoka H and Nakamura Y 2006 *J. Appl. Phys.* **99** 08G908
- [14] Wang J J, Sakurai T, Oikawa K, Ishida K, Kikuchi N, Okamoto S, Sato H, Shimatsu T and Kitakami O 2009 *J. Phys.: Condens. Matter* **21** 185008
- [15] Mai T K, Schoenstein F, Zighem F, Nowak S, Leridon B, Jouini N and Mercone S 2017 *J. Magn. Magn. Mater.* **422** 221
- [16] Leslie-Pelecky D L and Schalek R L 1999 *Phys. Rev. B* **59** 457
- [17] Sort J, Surinach S, Muñoz J S, Baró D, Nogués J, Chouteau G, Skumryev V and Hadjipanayis G C 2002 *Phys. Rev. B* **65** 174420
- [18] Gandha K, Elkins K, Poudyal N, Liu X and Ping Liu J P 2014 *Sci. Rep.* **4** 5345
- [19] Chakroune N, Viau G, Ricolleau C, Fievet-Vincent F and Fievet F 2003 *J. Mater. Chem.* **13** 312
- [20] Ung D, Soumare Y, Chakroune N, Viau G, Vaulay M J, Richard V and Fievet F 2007 *Chem. Mater.* **19** 2084
- [21] Soumare Y, Garcia C, Maurer T, Chaboussant G, Ott F, Fievet F, Piquemal J Y and Viau G 2009 *Adv. Funct. Mater.* **19** 1971
- [22] Mrad K, Schoenstein F, Nong H T T, Anagnostopoulou E, Mouton L, Mercone S, Jouini N, Viau G and Piquemal J Y 2017 *Crystal Growth and Design* (submitted)
- [23] Mercone S, Zighem F, Leridon B, Gaul A, Schoenstein F and Jouini N 2015 *J. Appl. Phys.* **117** 203905
- [24] Pousthomis M, Anagnostopoulou E, Panagiotopoulos I, Boubekri R, Fang W, Ott F, Ait Atmane K, Piquemal J Y, Lacroix L M and Viau G 2015 *Nano Res.* **8** 2231
- [25] Ott F, Maurer T, Chaboussant G, Soumare Y, Piquemal J Y and Viau G 2009 *J. Appl. Phys.* **105** 013915
- [26] Tannous C and Gieraltowski J 2008 *Eur. J. Phys.* **29** 475